



# Origins of non-equilibrium lithium isotopic fractionation in xenolithic peridotite minerals: Examples from Tanzania

Sonja Aulbach\*, Roberta L. Rudnick

Geochemistry Laboratory, Department of Geology, University of Maryland, College Park, MD 20742, U.S.A.

## ARTICLE INFO

### Article history:

Received 1 February 2008

Received in revised form 30 May 2008

Accepted 24 July 2008

### Keywords:

Lithium isotopes

Li diffusion

Isotopic disequilibrium

Kinetic isotope fractionation

Subsolidus Li redistribution

Metasomatism

Magma residence

Peridotite xenolith

## ABSTRACT

Olivine, clinopyroxene and orthopyroxene in variably metasomatised peridotite xenoliths from three lithospheric mantle sections beneath the East African Rift in Tanzania (Lashaine, Olmani, Labait) show systematic differences in their average Li concentrations (2.4 ppm, 2.0 ppm and 1.5 ppm, respectively) and intermineral isotopic fractionations, with olivine being heaviest ( $\delta^7\text{Li} = +2.3$  to  $+13.9\%$ , average  $+5.0\%$ ), followed by orthopyroxene ( $-4.1$  to  $+6.5\%$ , average  $+0.8\%$ ) and clinopyroxene ( $-6.7$  to  $+4.1\%$ , average  $-1.6\%$ ). These features are ascribed to the effects of kinetic Li isotope fractionation combined with different Li diffusivities in mantle minerals.

Two main mechanisms likely generate diffusion-driven kinetic Li isotope fractionation in mantle xenoliths (1) Li diffusion from grain boundary melt into minerals during recent metasomatism or entrainment in the host magma and (2) subsolidus intermineral Li-redistribution. The latter can produce both isotopically light (Li-addition) and heavy (Li-loss) minerals and may occur in response to changes in pressure and/or temperature.

Modelling shows that non-mantle-like  $\delta^7\text{Li}$  in clinopyroxene ( $<+2\%$ ), combined with apparent equilibrium olivine-clinopyroxene elemental partitioning in most peridotite xenoliths from all three Tanzanian localities probably reflects incipient Li addition during interaction with the host magma. Low  $\delta^7\text{Li}$  ( $<-3\%$ ), combined with high Li concentrations ( $>3$  ppm) in some clinopyroxene may require very recent (minutes) Li ingress from a Li-rich melt (100s of ppm) having mantle-like  $\delta^7\text{Li}$ . This might happen during late fragmentation of some mantle xenoliths caused by a volatile- (and Li-) rich component exsolved from the host basalt. In contrast, high Li concentrations ( $>2$  ppm) and  $\delta^7\text{Li}$  ( $>4\%$ ) in olivine from many Labait and Olmani samples are attributed to an older, pre-entrainment enrichment event during which isotopic equilibrium was attained and whose signature was not corrupted during xenolith entrainment. Low Li concentrations and mantle-like isotopic composition of olivine from most Lashaine xenoliths indicate limited metasomatic Li addition.

Thus, Li concentrations and isotope compositions of mantle peridotites worldwide may reflect two processes, with olivine mainly preserving a signature of depletion in refractory samples (low Li contents and  $\delta^7\text{Li}$ ) or of older (precursory) melt addition in metasomatised samples (high Li contents and  $\delta^7\text{Li}$ ), while non mantle-like, low  $\delta^7\text{Li}$  in almost all clinopyroxene can be due to Li ingress during transport in the host magma and/or slow cooling, if the samples were erupted in lavas. In Tanzania, the peridotites experienced rift-related heating prior to entrainment and were quenched upon eruption, so Li ingress is the most likely process responsible for the isotopically light clinopyroxene here.

© 2008 Elsevier B.V. All rights reserved.

## 1. Introduction

Lithium isotope geochemistry is increasingly being used to study deep-earth processes, in particular fluid–rock interactions and geochemical recycling, yet its behaviour during high-temperature processes and passage of fluids through the mantle, where Li is mildly incompatible, remains poorly understood. It is, however, clear that there is considerable variability of  $\delta^7\text{Li}$  (Li isotopic composition relative to L-SVEC standard:  $[(^{7}\text{Li}/^{6}\text{Li})_{\text{sample}}/(^{7}\text{Li}/^{6}\text{Li})_{\text{L-SVEC}} - 1] \times 1000$ ) in the

lithospheric mantle (40‰), which contrasts with the relatively uniform  $\delta^7\text{Li}$  of MORBs, which sample the convecting mantle ( $+2$  to  $+6\%$ , Chan et al., 1992; Moriguti and Nakamura, 1998a; Tomascak et al., 2008).

Equilibrium fractionation of lithium isotopes occurs in igneous systems at the low temperatures of pegmatite formation (Teng et al., 2006a), but not significantly at the high temperatures and high melt fraction of basalt differentiation ( $>1050$  °C; Tomascak et al., 1999). Therefore, it had originally been argued that Li isotopes could be used as a tracer of low-temperature modified slab-derived components and their dehydrated equivalents (Elliott et al., 2004; Nishio et al., 2004; Brooker et al., 2004), as different portions of the subducted oceanic crust have variable  $\delta^7\text{Li}$  due to interaction with seawater and metamorphic dehydration (Chan et al., 1992, 1994, 2002, 2006; Seyfried et al., 1998; Zack et al., 2003). However, recent experimental results and studies of

\* Corresponding author. Present address: University of Alberta, Earth and Atmospheric Sciences, ESB1-26, Edmonton, AB, T6G 2E3, Canada. Tel.: +1 780 492 8668; fax: +1 780 492 2030.

E-mail address: [aulbach@ualberta.ca](mailto:aulbach@ualberta.ca) (S. Aulbach).

contact aureoles, peridotites and phenocrysts in lavas indicate that Li isotopes can be strongly fractionated during high-temperature igneous processes due to diffusive kinetic fractionation (Richter et al., 2003; Lundstrom et al., 2005; Teng et al., 2006b; Beck et al., 2006; Jeffcoate et al., 2007; Rudnick and Ionov, 2007; Parkinson et al., 2007; Wagner and Delouie 2007; Tang et al., 2007; Marks et al., 2007; Aulbach et al., 2008; Ionov and Seitz, 2008). Thus, it is important to determine whether non-MORB-like  $\delta^7\text{Li}$  in mantle samples reflect kinetic effects or recycled crustal components.

Previous studies on peridotite xenoliths have reported a range of olivine-clinopyroxene Li isotope fractionation ( $\Delta^7\text{Li}^{\text{ol-cpx}}$ ) with both positive and negative signs (up to 3.5‰: Seitz et al., 2004; -2.4 to +1.2‰: Magna et al., 2006; -3.6 to +13.5‰: Jeffcoate et al., 2007; 3 to 23‰: Rudnick and Ionov 2007; 0.3 to 15.8‰: Wagner and Delouie 2007; 8.6 to 12.7‰: Tang et al., 2007; 24.2‰: Ionov and Seitz 2008). Although there are no experimental constraints on equilibrium Li isotope fractionation of mantle minerals at appropriate temperatures, very large inter-mineral fractionations are generally attributed to kinetic effects associated with Li ingress attending transport in the host magma or metasomatism immediately preceding entrainment. Other causes of kinetic Li isotope fractionation, in particular subsolidus inter-mineral Li re-distribution in response to changes in pressure or temperature, have received less attention (Tang et al., 2007; Ionov and Seitz, 2008).

We measured the Li isotopic composition of peridotitic olivine, orthopyroxene and clinopyroxene separates from well-studied xenoliths from two Tanzanian localities, Lashaine and Olmani, that have been affected by different styles of metasomatism, in addition to recent rift-related heating (Rudnick et al., 1993, 1994). We combine these data with those of minerals in peridotite xenoliths from the nearby Labait volcano (Aulbach et al., 2008) in order to determine the degree of isotopic fractionation between peridotite minerals and its origins and timing. Particular emphasis is placed on processes that may generate diffusive kinetic fractionation of Li isotopes in the lithospheric mantle and during entrainment of xenoliths in the host magma. For this purpose, we simultaneously model whole-grain Li concentrations and  $\delta^7\text{Li}$  using a nested sphere approach. Because many of the variables governing Li isotope behaviour are poorly constrained, our modelling provides only qualitative insights, awaiting a more comprehensive experimental dataset. Finally, we make some general observations on Li systematics combining data on all peridotite xenoliths reported in the literature so far.

## 2. Samples

The samples are well-documented mantle xenoliths retrieved from two Quaternary rift-related volcanoes in Tanzania: the Lashaine tuff cone, and the Olmani cinder cone (Dawson et al., 1970; Dawson, 1984; Cohen et al., 1984; Rudnick et al., 1993, 1994), which erupted in a part of the Mozambique fold belt that is interpreted as reworked craton (Möller et al., 1998). In contrast to kimberlite-hosted cratonic xenoliths, peridotites in the Tanzanian localities are not serpentinized and are generally quite fresh, although garnets are partially to fully replaced by kelyphite. Lashaine peridotites range from refractory garnet harzburgites and more fertile garnet lherzolites to metasomatised dunites and wehrlites. Clinopyroxenes show chemical zoning, interpreted as a young feature, and olivine inclusions within garnets have higher forsterite (Fo) contents than olivine in the matrix, attesting to an Fe enrichment event (Rudnick et al., 1994). The pressure-temperature array calculated from the compositions of minerals in garnet peridotites plots slightly above the 44 to 45 mW/m<sup>2</sup> model conductive geotherm (Rudnick et al., 1994).

Olmani peridotites have olivines with Fo up to 94, yet, with the exception of a refractory garnet harzburgite (89-773), they are also mostly clinopyroxene-bearing but orthopyroxene-free (dunites and wehrlites). All are LREE-enriched. The wehrlites may contain apatite, and have unusually high Ca/Al (up to 10.8 compared to 1.1 for chondrite) and Ti/Eu, consistent with interaction with a calcio-

carbonatite melt (Rudnick et al., 1993). The single harzburgite contains no Ca-rich phases, but does contain monazite, suggesting interaction with a Ca-free magnesio-carbonatite. The temperature range of Olmani peridotites is difficult to assess in the general absence of coexisting orthopyroxene-clinopyroxene, but when these two minerals do occur, calculated temperatures are similar to those from Lashaine peridotites, which could indicate a similar derivation depth if equilibrated to the same geotherm; alternatively, the Olmani peridotites may have last equilibrated to a higher geotherm related to East African Rift volcanism (Rudnick et al., 1993). Key characteristics of peridotites from Lashaine and Olmani are given in Table 1.

A third xenolith suite from Tanzania (Labait, on the margin of the Tanzanian craton) comprising silicate melt-metasomatised Fe-rich peridotites, garnet harzburgites and garnet lherzolites, and refractory garnet-free peridotites and spinel peridotites, has been previously described (Lee and Rudnick, 1999; Chesley et al., 1999), including their Li isotope systematics (Aulbach et al., 2008). These xenoliths are included here for completeness.

## 3. Analytical methods

Mineral dissolution and three-column Li purification for optically clean mineral separates is modified from the procedure of Moriguti and Nakamura (1998b), as described in Rudnick et al. (2004). Purified Li solutions were introduced into the Ar plasma using an auto-sampler and a CETAC Technologies MCN-6000 desolvating microconcentric nebulizer, and measured on the Nu Plasma MC-ICPMS in the Geochemistry Laboratory at the University of Maryland, using the standard bracketing

**Table 1**  
Key parameters for Lashaine and Olmani peridotites

Sample	Rock type	Mineral	Mode	Grain size	Mg#	T <sub>Ca-in-opx</sub>	
<i>Lashaine</i>							
89-661	gt lherz	refr	ol	86.9	3	93.3	1090
		opx		6.1	3	93.7	
89-664	gt harz*	f/m	cpx	0.8	0.1	89.2	1230
		opx		9.7	4	91.9	
89-669	wehr*	f/m	ol	86.0	2	88.2	1040
		cpx		8.6	0.3	89.5	
		opx		0.9	0.3	88.9	
89-671	dunite*	f/m	ol	95.2	0.5	87.0	na
89-672	dunite	f/m	ol	96.2	5	92.5	1110
		cpx		3.8	1.5	93.0	
		opx		trace	0.02	93.6	
89-674	gt lherz*	f/m	ol	79.7	4	91.2	1250
		cpx		5.8	0.5	89.9	
		opx		11.4	2	92.7	
89-675	gt harz	refr	ol	72.2	2	92.4	1240
		opx		24.0	1.5	93.3	
89-680	gt harz	refr	ol	72.7	1.5	93.0	1150
		cpx		2.8	0.5	93.0	
		opx		20.4	0.5	93.5	
89-719	gt harz	refr	ol	82.9	7	92.7	1150
		cpx		1.2	0.3	93.8	
		opx		11.5	3	93.7	
<i>Olmani</i>							
89-772	dunite	f/m	ol	96.5	1.5	87.6	950
		cpx		3.4	0.2	88.0	
89-773	harz	refr	ol	82.0	3	93.6	1080
		opx		17.5	1	94.2	
89-774	dunite*	f/m	ol	99.1	7	93.5	na
89-776	dunite	f/m	ol	97.2	2	94.4	1120
		cpx		3.3	1	94.0	
89-777	wehrlite	f/m	ol	91.9	2.5	94.2	1120
		cpx		6.9	0.5	93.0	
89-778	dunite	f/m	ol	98.2	5	91.3	na

\*Contains phlogopite. Data from Rudnick et al. (1994). Rock types (gt garnet, lherz lherzolite, harz harzburgite) distinguished according to whether sample is refractory (refr) or fertile/metasomatised (f/m). Ol olivine, opx orthopyroxene, cpx clinopyroxene. Modes in vol.%, grain size in mm, T<sub>Ca-in-opx</sub> (Brey et al., 1990) in °C; Mg# is 100 Mg/(Mg+Fe).

method (Tomascak et al., 1999). Lithium concentrations were estimated in the course of Li isotope measurements by comparison of sample signal intensities with those obtained from a 50 ppb solution of the NIST L-SVEC standard and adjusting for sample weight. The estimated 2 sigma uncertainty of this method is ~10% (Teng et al., 2004). The details of sample introduction and mass spectrometry are given in Tomascak et al. (1999), Rudnick et al. (2004) and Teng et al. (2004).

Analyses of international rock standards and pure Li standard solutions performed during the course of these analyses yielded concentrations and  $\delta^7\text{Li}$  values consistent with previously published data. In comparison with Li concentrations reported in Govindaraju (1995) and Eggins et al. (1997), we obtained 13.9 ppm for BCR-1 (cf. 14 ppm), 4.8 ppm for BHVO-1 (cf. 4.9 ppm) and 23.9 ppm for UB-N (cf. 27 ppm). The  $\delta^7\text{Li}$  values for pure Li in-house standard UMD-1 and IRMM-016 (average  $\delta^7\text{Li}$  of  $54.6 \pm 0.8\%$  ( $n=27$ ) and  $0.2 \pm 1\%$  ( $n=17$ )  $2\sigma$ , respectively) and international rock standards agree within uncertainty with previously published values (BHVO-1:  $4.5 \pm 1\%$ ,  $n=8$ , cf. 4.3 to 5.8%; BCR-1:  $3.0 \pm 0.5\%$ ,  $n=4$ , cf. 2.0 to 2.7%; UB-N:  $-1.8 \pm 0.9\%$ ,  $n=4$ , cf.  $-2.6$  to  $-2.7\%$ ; all uncertainties reported at the 2 sigma level) as summarized by Aulbach et al. (2008). The external precision ( $2\sigma$  on repeat runs) is generally  $\leq 1\%$  based on long-term analyses of the UMD-1 and IRMM-016 pure Li standards (Teng et al., 2004).

## 4. Results

### 4.1. Lithium concentrations

Lithium concentrations and apparent distribution coefficients, as well as bulk rocks reconstructed from minerals using mineral modes reported in Rudnick et al. (1994) and Lee and Rudnick (1999), are given

in Table 2. Combined with results from Labait (Aulbach et al., 2008), Li concentrations in olivine vary from 0.6 to 4.8 ppm (average 2.4 ppm). With the exception of the single wehrlite (sample 89-669, which has 2.7 ppm Li in olivine), olivines from Lashaine peridotites have low Li concentrations ( $\leq 1.7$  ppm, averaging  $1.2 \pm 0.4$  ppm), similar to those expected for depleted or primitive upper mantle (Jagoutz et al., 1979; Ryan and Langmuir, 1987; McDonough and Sun, 1995; Seitz and Woodland, 2000). In contrast, Li contents in olivines from the Olmani dunites and wehrlites are generally much higher ( $\leq 4.1$  ppm, averaging  $3.3 \pm 0.6$  ppm). However, olivine in the single monazite-bearing harzburgite from Olmani (89-773) has markedly lower Li concentration (0.7 ppm). For comparison, at Labait, olivines from silicate melt-metasomatised Fe-rich peridotites have the highest Li concentrations observed for Tanzanian peridotites (average  $4.1 \pm 0.8$ ), followed by those from garnet harzburgites, garnet lherzolite and refractory garnet-free peridotites. Spinel peridotites from Labait have olivines with the lowest Li concentrations ( $\leq 1.9$  ppm) for that locality.

Lithium concentrations in clinopyroxenes vary from 0.5 to 4.4 ppm (average 2.0 ppm) and those in orthopyroxene from 0.6 to 3.8 ppm (average 1.5 ppm). Clinopyroxenes from Lashaine have relatively low concentrations ( $\leq 2.2$  ppm, averaging  $1.5 \pm 0.6$  ppm), with the exception of clinopyroxene in the wehrlite (89-669), which, like the olivine from this sample, has a high Li concentration (3.6 ppm). Interestingly, the coexisting orthopyroxene has low Li concentration, similar to orthopyroxene from garnet harzburgites (~1 ppm), while orthopyroxenes in garnet lherzolites have the highest Li concentrations (2.1 and 2.2 ppm). Clinopyroxenes in the dunites and wehrlites from Olmani have low Li concentrations ( $\leq 1.9$  ppm) compared to coexisting olivine. The monazite-bearing harzburgite in the Olmani sample suite (89-773) is the only orthopyroxene-bearing sample from that location and its

**Table 2**

Li concentrations, partitioning, Li isotope compositions and intermineral fractionations of peridotitic mineral separates from Tanzania

Sample name	Rock type	Li (ppm)			$K_D$			$\delta^7\text{Li}$			$\Delta^7\text{Li}$			Calc whole rock		
		ol	cpx	opx	ol/cpx	ol/opx	cpx/opx	ol	cpx	opx	ol-cpx	ol-opx	opx-cpx	Li (ppm)	$\delta^7\text{Li}$	
<i>Lashaine</i>																
89-661	gt lherz	0.7		2.1		0.3									na	na
89-664	gt harz		1.4	1.4											na	na
89-669	wehrlite	2.7	3.6	1.0	0.8	2.7	3.6	na	-3.2 (4)	6.5 (1)				9.7	2.6	na
89-671	dunite	1.7						13.9 (3)							na	na
89-672	dunite	1.1	1.6	0.9	0.7	1.2	1.8	4.2 (2)	0.4 (4)	-2.5 (2)	3.8	6.7	-2.9	1.1	4.1	
89-674	gt lherz	1.5	2.2		0.7			5.0 (2)		2.3 (2)		2.7		na	na	
89-675	gt harz	0.6		1.0		0.6				-3.2 (2)				na	na	
89-680	gt harz	1.5	0.9	1.0	1.7	1.5	0.9	2.3 (3)	-1.5 (2)	1.6 (2)	3.9	0.7	3.1	1.3	2.0	
89-719	gt harz	1.1	1.2	0.8	0.9	1.4	1.5	2.8 (3)	-3.9 (1)	0.0 (1)	6.7	2.9	3.9	1.0	2.3	
<i>Olmani</i>																
89-772	dunite	4.1	1.5		2.7			4.1 (3)	-2.0 (2)		6.1			4.0	3.9	
89-773	harz	0.7		0.6		1.2		3.0 (4)		0.0 (1)		3.0		0.7	2.5	
89-774	dunite	3.0						3.3 (4)						na	na	
89-776	dunite	3.7	1.6		2.3			6.2 (5)	-0.4 (1)		6.6			3.6	6.0	
89-777	wehrlite	3.5	1.9		1.8			5.7 (3)	-1.4 (2)		7.2			3.3	5.1	
89-778	dunite	2.6						9.3 (1)						na	na	
<i>Labait</i>																
KAT-17	gt harz	3.4	2.2	0.8	1.5	4.3	2.8	4.7	-0.3	3.2	5.0	1.5	3.5	2.7	4.1	
LB-4	gt harz	2.3	1.2	1.2	1.9	1.9	1.0	4.7	-2.6	1.2	7.3	3.6	3.8	1.9	3.4	
LB-6	gt-free perid	1.9		1.9		1.0		3.7		-4.1		7.9		na	na	
LB-17	gt-free perid	2.7						4.0						na	na	
LB-21	gt-free perid	2.2	3.8	1.5	0.6	1.5	2.5	2.5	-4.9	1.1	7.4	1.4	6.0	2.3	2.2	
LB-29	sp perid	1.9		1.2		1.6		3.4		3.5		-0.1		1.7	3.4	
LB-31	sp perid	1.8	0.9	1.5	2.0	2.0	0.6	3.3	1.5		1.8			1.6	na	
LB-45	gt lherz	2.4	2.0	2.5	1.2	1.0	0.8	4.7	0.1	0.7	4.6	4.0	0.6	2.0	2.9	
LB-46	Fe-rich perid	4.4	3.0	3.8	1.5	1.2	0.8	5.2	-6.7	-1.8	11.9	7.0	4.9	4.2	3.7	
LB-51	Fe-rich perid	4.8	4.4		1.1			6.6	4.1		2.4			4.7	6.3	
LB-59	Fe-rich perid	3.2						6.6						na	na	

Ol olivine, opx orthopyroxene, cpx clinopyroxene, gt garnet, lherz lherzolite, harz harzburgite, perid peridotite; apparent distribution coefficients ( $K_D$ ) are also shown.  $\delta^7\text{Li}$  in ‰, numbers in parentheses are numbers of replicates and/or duplicates; 89-661 opx, 89-772 cpx and 89-774 olivine reproduced within 1.2‰ uncertainty, all others within 1‰. Intermineral isotope fractionation ( $\Delta^7\text{Li}_{\text{mineral A-mineral B}}$ ) is also given. Concentrations and Li isotope data for Labait peridotites from Aulbach et al. (2008). Whole rocks are calculated from modes given in Table 1 and in Lee and Rudnick (1999) where all major Li hosts were analysed, and assuming that Li concentrations in garnets, where applicable, are negligible.

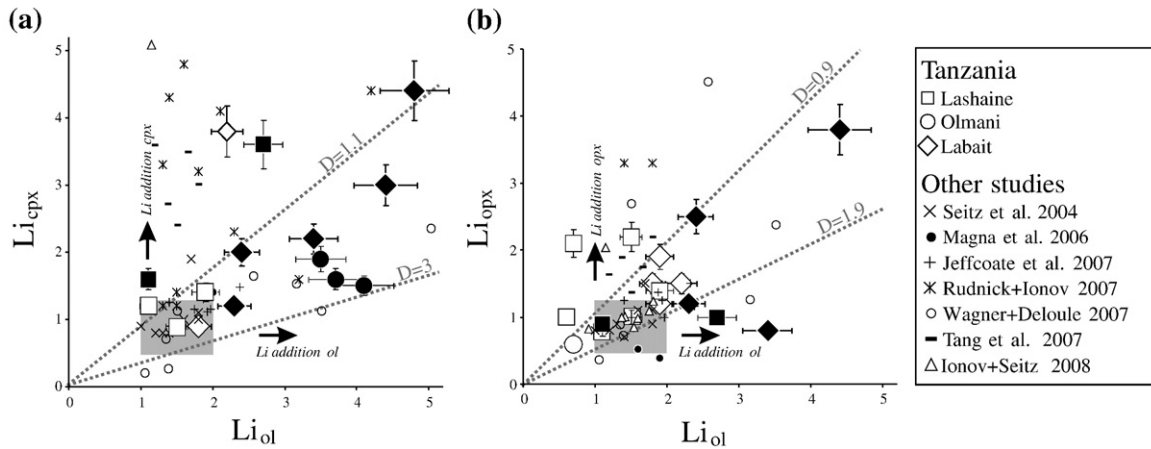


**Fig. 1.** Li concentrations (ppm) in olivine vs. (a) clinopyroxene and (b) orthopyroxene (open symbols: refractory, filled symbols: fertile/metasomatised peridotites). Shown for comparison are results for peridotite xenoliths reported in the literature (Seitz et al., 2004: San Carlos, Arizona, Eifel volcanic field, Vitim, Siberia and Kapfenstein, Austria; Magna et al., 2006: San Carlos, Vitim, Atsagin-Dush, Tariat; Jeffcoate et al., 2007: Vitim, Tariat and Dariganga, Central Asian Orogenic Belt; Rudnick and Ionov, 2007: Tok, Barhatny and Kappy, SE Siberian Craton; Wagner and Deloule, 2007: Massif Central; Tang et al., 2007: Hannuoba, North China Craton; Ionov and Seitz, 2008: Kamchatka, Vitim). Grey fields show Li concentrations and dotted lines show partition coefficients in equilibrated, unmetasomatised peridotites (Brenan et al., 1998; Eggins et al., 1998; Seitz and Woodland, 2000; Adam and Green, 2006); higher Li contents are ascribed to metasomatic Li addition.

orthopyroxene has the lowest Li concentration of all minerals measured in this study (0.6 ppm). For comparison, clinopyroxenes and orthopyroxenes in Fe-rich peridotites from Labait have high Li concentrations (3.0 to 4.4 ppm and 3.8 ppm, respectively), whereas those in clinopyroxene and orthopyroxene in the other Labait peridotites are lower, overlapping the concentrations seen for these minerals from the other localities. Orthopyroxene in a garnet harzburgite (KAT-17) has the lowest Li concentration (0.8 ppm) of any mineral from this locality.

In general, Li concentrations in olivine exceed those in clinopyroxene and orthopyroxene. The majority of apparent distribution coefficients for Li between olivine and clinopyroxene ( $^{ol/cpx}K_{D(Li)}$ ) and olivine and orthopyroxene fall between 1 and 2, which is similar to suggested equilibrium partitioning values of 1.1 to 3 for  $^{ol/cpx}K_{D(Li)}$  (Brenan et al., 1998; Eggins et al., 1998; Seitz and Woodland, 2000; Adam and Green, 2006) and between 0.9 to 1.9 for  $^{ol/opyx}D_{D(Li)}$  (Fig. 1). Thus, while Li is enriched in most of the minerals relative to primitive upper mantle (grey boxes in Fig. 1), most also appear to be equilibrated with respect to Li concentration.

#### 4.2. Lithium Isotopic Compositions

Mineral and reconstructed bulk rock lithium isotopic compositions ( $\delta^7Li$ ), as well as intermineral isotope fractionations ( $\Delta^7Li_{\text{mineralA-mineralB}}$ )

are reported in Table 2 (for the full dataset, including duplicates and replicates, see Appendix 1) and plotted in Fig. 2. Two trends are apparent from the data: 1) intermineral fractionations are consistent in sign from locality to locality, with olivine systematically heavier than coexisting clinopyroxene or orthopyroxene, though the magnitude of the fractionation is variable and 2) olivines in Li-rich, more strongly metasomatised xenoliths are isotopically heavier than their counterparts in less metasomatised and Li-poor, refractory xenoliths. Each of these features is described in the following paragraphs.

In peridotites from Lashaine and Olmani, the  $\delta^7Li$  of olivine is heavier (range: +2.3 to +13.9, average +5.5‰) than that of coexisting clinopyroxene (range: -3.9 to +0.4, average -1.8‰) in all samples and, with one exception,  $\delta^7Li$  of olivine is also heavier than that of coexisting orthopyroxene (range: -2.5 to +6.5, average +1.0). In addition, the  $\delta^7Li$  of orthopyroxene, with one exception (89-672), is heavier than that of coexisting clinopyroxene (Table 2). The Labait samples show similar systematics (Aulbach et al., 2008). Including the data from Labait, the average intermineral isotope fractionation is as follows:  $\Delta^7Li_{ol-cpx} = +5.7\text{‰}$  (range 3.8 to 7.2),  $\Delta^7Li_{ol-opx} = +3.2\text{‰}$  (range 0.7 to 6.7) and  $\Delta^7Li_{opx-cpx} = +3.6\text{‰}$  (range -2.9 to 9.7).

There is a general correlation between the degree of metasomatism/fertility of the peridotites and the  $\delta^7Li$  and Li ppm of their olivines. The  $\delta^7Li$  of olivines in the two garnet harzburgites from Lashaine (89-

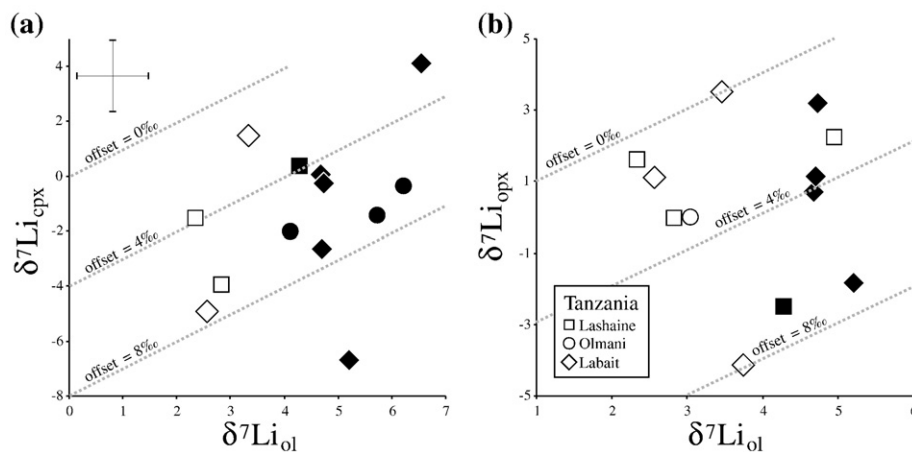


**Fig. 2.**  $\delta^7Li$  (in ‰) in olivine plotted against (a)  $\delta^7Li$  in clinopyroxene and (b)  $\delta^7Li$  in orthopyroxene (open symbols: refractory, filled symbols: metasomatised). Lines of constant isotopic offset are also shown. Two sigma error bars on measurement is plotted in the upper left of panel a.

680, 89–719) are lower (+2.3 and +2.8) than in more fertile or metasomatised samples (Fe-rich dunite, 89–671: +13.9; clinopyroxene dunite, 89–672: +4.2, phlogopite-garnet lherzolite, 89–674: +5.0), although for this locality, Li content in olivine is not significantly different between the refractory and metasomatised/fertile samples. Olivines in dunites and a wehrilite from Olmani, which are interpreted to have formed by interaction between refractory harzburgite and calcio-carbonatite (Rudnick et al., 1993) tend to have higher  $\delta^7\text{Li}$  (+3.3 to +9.3) and higher Li concentrations, compared to that of harzburgite 89–773, which has the lowest  $\delta^7\text{Li}$  (+3.0) and Li content (0.7 ppm) of all measured samples from this locality. These trends are similar to those seen previously in Labait xenoliths, where olivines in metasomatised Fe-rich peridotites have the highest  $\delta^7\text{Li}$  (+5.2 to +6.6) and Li content, whereas those in refractory spinel peridotites and garnet-free peridotites have lower  $\delta^7\text{Li}$  (+2.6 to +4.6) and Li content.

## 5. Modelling

The isotopic variability observed here between coexisting minerals in peridotite xenoliths likely reflects disequilibrium processes, as documented in numerous recent studies (Jeffcoate et al., 2007; Rudnick and Ionov, 2007; Tang et al., 2007; Ionov and Seitz, 2008; Aulbach et al., 2008). In order to understand what conditions are necessary to produce the observed compositions in the Tanzanian xenoliths, we model Li diffusion, as described below.

### 5.1. Approach

Lithium isotopic fractionation between two minerals can be calculated for the simple case of one-dimensional diffusion, assuming an infinite reservoir of Li at the surface of each mineral and that the minerals act as semi-infinite reservoirs, using Fick's second law (Crank, 1975):  $\frac{C_x - C_1}{C_0 - C_1} = \text{erfc} \left[ \frac{x}{2\sqrt{Dt}} \right]$ , where  $C_x$  is the Li concentration at distance  $x$  (here: radius of a nested sphere) in the modelled phase,  $C_1$  is the original element concentration (here: initial mineral core),  $C_0$  is the Li concentration at the surface (here mineral rim),  $\text{erfc}$  is the error function,  $D$  is the diffusion coefficient and  $t$  is time. The differential mobility of  $^7\text{Li}$  and  $^6\text{Li}$ , which causes isotopic fractionation, is linked to the empirically determined exponent,  $\beta$ , where the ratio of the diffusion coefficients of two isotopes are related as follows:  $D_{7\text{Li}}/D_{6\text{Li}} = (m_{6\text{Li}}/m_{7\text{Li}})^\beta$ , where  $m$  is mass (Richter et al., 2003). We allow  $C_0$  and  $C_1$  to vary (as discussed below) in order to fit the observations; justification for the choice of other parameters adopted here (e.g.,  $\beta$ ,  $D$ ,  $\delta^7\text{Li}$  of the source of Li,  $x$ ) is provided in section 5.3.

The surface concentration is taken to be the concentration of the mineral rim, which is dictated by the equilibrium partition coefficient ( $K_D$ ) between the rim and a fluid or neighbouring mineral grain with which it is in contact. For  $K_D \neq 1$  the concentration of the rim will therefore be different from that of a fluid or touching mineral. It is the concentration ratio between mineral rim and core that, together with  $\beta$ , governs the degree of isotopic fractionation produced.

In the present study,  $\delta^7\text{Li}$  is measured on dissolved mineral separates, and thus  $\delta^7\text{Li}$  is averaged over the whole grain and will not reflect the maximum intermineral Li isotope fractionation attained at the grain scale where intra-grain  $\delta^7\text{Li}$  variations are likely, as demonstrated by *in situ* studies (Beck et al., 2006; Jeffcoate et al., 2007; Parkinson et al., 2007; Wagner and Deloule 2007; Tang et al., 2007). Therefore, it is necessary to integrate  $\delta^7\text{Li}$  for the whole grain. We use a nested-spheres approach (100 spheres per mineral grain) to determine the bulk Li content and  $\delta^7\text{Li}$  for hypothetical spherical grains ( $x=r$ ). This approach assumes that Li is added simultaneously to minerals from grain boundaries (instead of volume diffusion) and does not account for the possibility that there may be gradients across a sample (xenolith in the host basalt, or mantle wall rock next to a melt conduit) where the rocks closest to the edge or contact will be affected by Li addition earlier and longer than samples further removed from the edge or contact.

### 5.2. Limitations

Fully quantitative modelling is hampered by our lack of knowledge of: (1) the value of  $\beta$  in peridotite minerals; (2) the diffusivity of Li in olivine; (3) the dependence of diffusivity on (i) crystallographic orientation (e.g., Kohlstedt and Mackwell, 1999), (ii) oxygen and water fugacity (which enhance crystallographic defects and thus diffusivity; e.g., Chakraborty, 1997; Hier-Majumder et al., 2005), (iii) substitution type (e.g., exchange with FeMg vs vacancies; S. Klemme, pers. comm.), (iv) diffusion mechanism (volume, grain boundary, defect, multi-path diffusion or combinations thereof; Farver et al., 1994; Watson and Baxter, 2007), (v) metasomatic style (Seitz and Woodland, 2000; Woodland et al., 2004; Rudnick and Ionov, 2007); (4) pre-diffusion (initial) compositions; (5) effects of peridotite distance from an external Li source (for magma conduits or veins) or xenolith fragmentation in the host magma and resultant superposition of Li diffusion profiles and of deviations of grain shapes from the ideal sphere.

Considering the uncertainties regarding the influence of the many factors governing Li diffusivity and associated isotope fractionation, the simple modelling approach outlined above is deemed sufficient to obtain a qualitative, at best a semi-quantitative sense of the degree and timing of Li isotope fractionation in peridotite xenoliths. We approach the problem in two ways: (1) a qualitative exploration of the effects of various parameters (see section 5.4) and (2) determining a specific set of parameters intended to reproduce the Li- $\delta^7\text{Li}$  measured in peridotite xenoliths (Appendices 2 and 3).

### 5.3. Choice of modelling parameters

To model Li addition during igneous processes, we focus on olivine and clinopyroxene since olivine is the major mineralogical constituent of the samples and because diffusivity of Li is available for clinopyroxene but not orthopyroxene. Specific values are assumed for the different parameters controlling  $\delta^7\text{Li}$  fractionation, as described below, except where a given parameter was explicitly varied to assess its effect on Li isotope behaviour.

*Li Diffusivity (D):* Assuming that the measured diffusivities of Li in diopside determined by Coogan et al. (2005) as a function of temperature are appropriate for the Cr-diopsides in mantle xenoliths, the diffusivity of Li in clinopyroxene at temperatures of last equilibration (Rudnick et al., 1993, 1994; Lee and Rudnick, 1999) was calculated from their algorithm. To model Li ingress during entrainment we assume a temperature of 1300 °C ( $D = 7.9 \cdot 10^{-11} \text{ m}^2 \text{ s}^{-1}$ ), which is above the solidus temperature of alkali basalt at 5 GPa (Tsuruta and Takahashi, 1998).

*Beta* has been estimated to be 0.215 in silicate melts (Richter et al., 2003), 0.12 in amphibolites (Teng et al., 2006b) and 0.15 to 0.27 in phenocrysts surrounded by groundmass (Beck et al., 2006; Parkinson et al., 2007). We adopt an intermediate value of 0.2 for our modelling.

*Grain size:* The mineral radius  $x$  is set to 3 mm for olivine and 1 mm for clinopyroxene, which is similar to some samples in this study (Vauchez et al., 2005; Table 1) and other peridotite xenolith suites (authors' personal observation). Actual values are used where modelling is aimed at reproducing measured values (Table 1, Appendix 3).

*Values for  $^{ol/cpx}K_{DLi}$*  range from 1.1 to 3 (Brenan et al., 1998; Eggins et al., 1998; Adam and Green, 2006); we adopt a value of 2 (ignoring possible pressure and temperature effects on partitioning).

*$\delta^7\text{Li}$  of the source of Li:* Because there is no evidence for mantle-derived melts or fluids having  $\delta^7\text{Li}$  significantly  $< 0\%$  (see Tomascak, 2004, and references therein), for most clinopyroxenes, simple equilibration with a low- $\delta^7\text{Li}$  melt can be excluded and isotope fractionation during Li influx is required to obtain very low  $\delta^7\text{Li}$  (i.e.  $C_0 > C_1$ ). Nevertheless, the lower the  $\delta^7\text{Li}$  of the fluid, the less the concentration contrast ( $C_0/C_1$ ) required to obtain low  $\delta^7\text{Li}$  and the longer the time it takes to reach the minimum  $\delta^7\text{Li}$  value (see section

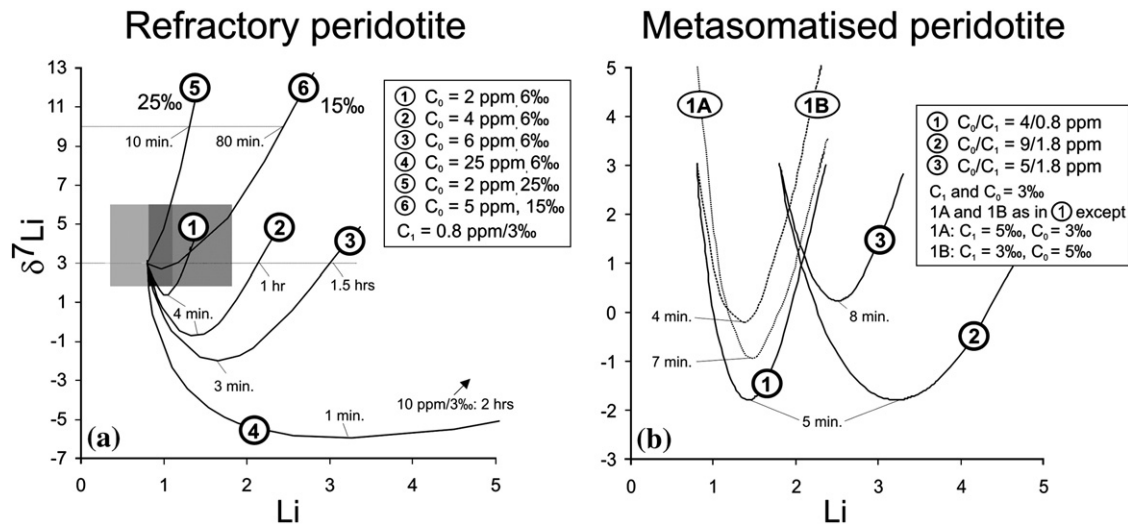


**Fig. 3.** Modeled trajectories of lithium concentrations (ppm) against  $\delta^7\text{Li}$  for whole mineral grains experiencing Li ingress in a) refractory peridotite and b) metasomatised peridotite. Each curve represents the pathway of a mineral with elapsed time. In all examples diffusivity =  $7.9 \times 10^{-11} \text{ m}^2\text{s}^{-1}$ , which corresponds to a temperature of 1300 °C for clinopyroxene,  $\beta=0.2$  and  $x=1 \text{ mm}$ . (a)  $C_0$  is varied to produce trajectories encompassing most of the values reported in the literature and shown in Fig. 4. The approximate times needed to produce  $\delta^7\text{Li}$  troughs and higher values are indicated. (b) Illustration of the response of trajectory 1 to increasing rim composition ( $C_0$ ) at constant  $C_0/C_1$  (trajectory 2) and at constant  $C_0-C_1$  (trajectory 3), and to higher initial  $\delta^7\text{Li}$  (trajectory 1A) and higher rim  $\delta^7\text{Li}$  (trajectory 1B), all other parameters being equal. A change in diffusivity ( $D$ ) or grain size ( $x$ ) produces identical curves but different times for each composition. Grey fields show range of “normal” mantle concentrations (references as in Fig. 1) and  $\delta^7\text{Li}$  (Chan et al., 1992; Moriguti and Nakamura, 1998a; Tomascak et al., 2008) for clinopyroxene (light grey) and olivine (dark grey), which partially overlap.

5.4). For example, if  $C_0$  has a value of 0 instead of 6‰ and all other parameters as shown in Fig. 3, example 4, then a  $\delta^7\text{Li}$  of  $-5.1\text{‰}$  takes 5 min instead of 1 min to reach. However, if we assume that the low  $\delta^7\text{Li}$  in xenolithic clinopyroxene reflects late fluid ingress from the host magma, as suggested previously (e.g., Rudnick and Ionov, 2007), then in the case of Labait the host melilitite is known to have a mildly elevated  $\delta^7\text{Li}$  of ca +5‰ (Aulbach et al., 2008), which is why we chose a similar value to model Li ingress.

More details on the choice of modelling parameters and some examples from the dataset can be found in Electronic Appendices 2 and 3.

#### 5.4. General features of whole grain Li- $\delta^7\text{Li}$ evolution

Figure 3a shows how Li concentration and  $\delta^7\text{Li}$  of minerals change with time and as a function of the concentration ratio between rim ( $C_0$ ) and core ( $C_1$ ). With increasing  $C_0/C_1$ , and all other parameters held constant, both the minimum  $\delta^7\text{Li}$  and time at which the trough

composition is reached decrease (Fig. 3a, examples 1–4). In addition, the slope of the curve is steeper prior to reaching the trough (down-going limb) compared to that subsequent to the trough (up-going limb). Hence, for increasing rim-core concentration ratios, the lowest isotope compositions are reached quickly relative to the time it takes for isotopic equilibration to be completed, and Li- $\delta^7\text{Li}$  evolution curves become increasingly asymmetric. These four curves encompass most of the clinopyroxene data from our study and many of the olivine compositions (Fig. 4). Similar to changing  $C_0/C_1$ , a choice of lower and higher  $\beta$  entails smaller and larger maximal  $\delta^7\text{Li}$  fractionations, respectively, the degree of which depends on the  $C_0/C_1$  used in the modelling. For identical  $\delta^7\text{Li}$  of core and rim (e.g., 5‰) and  $C_0/C_1=2$  (or 4), the maximum  $\delta^7\text{Li}$  decrease for a  $\beta$  of 0.1 is ca 0.7 (or 1.9)‰, for a  $\beta$  of 0.2 it is 1.7 (or 4.0)‰ and for a  $\beta$  of 0.3 it is 2.7 (or 6.1)‰.

In order to produce the high  $\delta^7\text{Li}$  and small amounts of Li gain seen in some olivines (89-669 from Lashaine and 89-776 from Olmani),  $C_0/C_1$  must be small and the  $\delta^7\text{Li}$  of the rim (hence source of Li) must be very high (e.g., 25‰) (Fig. 3a, example 5, Fig. 4); higher  $C_0$  and somewhat

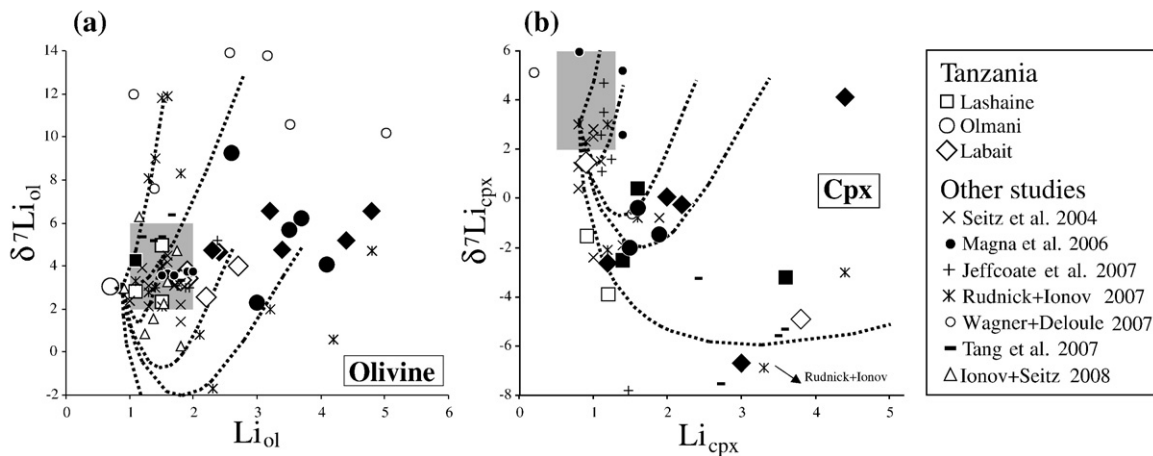


**Fig. 4.** Lithium concentrations (ppm) versus  $\delta^7\text{Li}$  (‰) for (a) olivine and (b) clinopyroxene (large open symbols: refractory, large filled symbols: metasomatised) from Tanzanian peridotite xenoliths plotted against five of the modeled trends of Li- $\delta^7\text{Li}$  evolution and “normal” mantle fields shown in Fig. 3a. Data for peridotite xenoliths from other studies as in Fig. 1; normal mantle range as in Figs. 1 and 3.

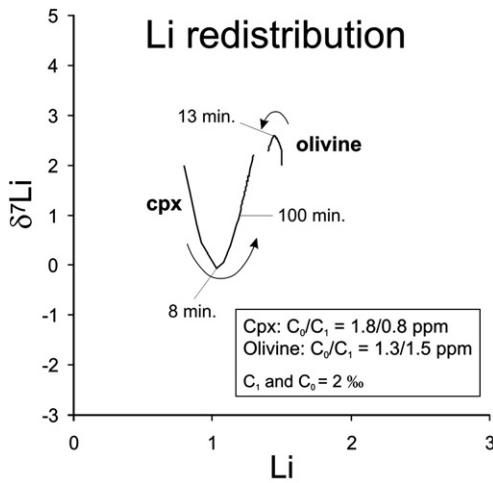


Fig. 5. As in Fig. 3, but illustrating Li- $\delta^7\text{Li}$  during moderate Li gain in clinopyroxene and small Li loss in olivine, such as might be expected during intermineral Li redistribution.

lower  $\delta^7\text{Li}$  are required to produce high  $\delta^7\text{Li}$  with greater Li gain (example 6, Figs. 3a and 4). The effect of changing  $\delta^7\text{Li}$  of the initial and rim value is also illustrated in Fig. 3b (examples 1, 1A and 1B): higher initial  $\delta^7\text{Li}$  at constant rim  $\delta^7\text{Li}$  (example 1A) will produce a stronger relative  $\delta^7\text{Li}$  fractionation at higher minimum  $\delta^7\text{Li}$ , while higher rim  $\delta^7\text{Li}$  at constant initial  $\delta^7\text{Li}$  (example 1B) will produce a weaker relative  $\delta^7\text{Li}$  fractionation at higher minimum  $\delta^7\text{Li}$ .

To model Li ingress during entrainment into previously metasomatised and hence Li-rich samples,  $C_1$  must increase. Because the ratio of rim to core Li concentration  $C_0/C_1$  determines the degree of isotope fractionation (at constant  $\beta$ ), changing the  $C_1$  from 0.8 ppm (typical of refractory, unmetasomatised clinopyroxene) to 1.8 ppm (a more typical value for metasomatised clinopyroxene) requires the new  $C_0$  to be 9 ppm in order to maintain the same degree of  $\delta^7\text{Li}$  decrease (Fig. 3b, examples 1 and 2: down to  $-1.8\%$ ). The slope of the evolution curve (rate of  $\delta^7\text{Li}$  change per ppm Li increase) is lower for the second example, which has the higher  $C_0$ .

Due to the similar Li- $\delta^7\text{Li}$  initial trajectories for a range of  $C_0/C_1$  (downgoing limb in Fig. 3, examples 1 to 4) the range of possible rim concentrations that can reproduce measured values within the analytical uncertainties (10% for concentrations, 1% for  $\delta^7\text{Li}$ ) is larger

for samples that experienced a smaller Li gain than for samples that experienced a larger Li gain.

Finally, Fig. 5 illustrates the effect of redistribution of Li from one mineral (e.g., olivine), which becomes temporarily isotopically heavier, into another mineral (e.g., clinopyroxene), which becomes temporarily lighter, corresponding to a decrease in apparent  $^{ol/cpx}K_D$  (in this example  $^{ol/cpx}K_D$  changes from 1.9 (1.5/0.8 ppm) to 0.7 (1.3/1.8 ppm)). Such a change in  $K_D$  might reflect the effects of changing temperature (e.g., Ionov and Seitz, 2008, suggested  $K_D$  decreases dramatically with falling temperature). The ratio  $C_0/C_1$  of the mineral gaining Li (1.8/0.8 ppm) is far greater than that of the mineral losing Li (1.3/1.5 ppm), which produces a stronger  $\delta^7\text{Li}$  fractionation.

Changing diffusivity and relative grain sizes will affect the amount of intermineral Li isotope fractionation produced during Li ingress. Because olivine in peridotites is usually larger than clinopyroxene (depending on the degree of deformation; Vauchez et al., 2005; see also Table 1 and photomicrographs in the electronic supplement) and Li diffusivity is presumed to be slower in olivine than clinopyroxene (see section 6.2), the change in Li concentration and  $\delta^7\text{Li}$  in olivine lags behind that in clinopyroxene. These effects are illustrated in Fig. 6. Increasing olivine grain size from 3 to 5 mm, all other parameters being held constant, leads to an increase in  $\Delta^7\text{Li}^{ol-cpx}$  with a maximum at time  $t_1$  (Li ingress into clinopyroxene, but olivine is barely affected),  $\Delta^7\text{Li}^{ol-cpx} = 0$  at time  $t_2$  and a minimum  $\Delta^7\text{Li}^{ol-cpx}$  at time  $t_3$  (Li ingress into olivine, Li isotope relaxation in clinopyroxene) (Fig. 6a, curve 1). Increasing the grain size contrast leads to increasing  $t_x$  (Fig. 6a, curve 2). The effect of lowering Li diffusivity in olivine from one to two orders of magnitude relative to that in clinopyroxene, assuming identical grain sizes, is similar to that of increasing grain size contrast, but it takes longer for  $t_x$  to be attained (Fig. 6b, curves 1 and 2). Combining the effects of grain size and diffusivity differences by assuming a 5 mm grain size for olivine, 1 mm for clinopyroxene, a Li diffusivity in clinopyroxene of  $7.9 \times 10^{-11} \text{ m}^2\text{s}^{-1}$  and two orders of magnitude lower diffusivity in olivine, all other parameters being held constant, as described above, will lead to a maximum  $\Delta^7\text{Li}^{ol-cpx}$  of ca +4‰ after minutes,  $\Delta^7\text{Li}^{ol-cpx}$  of ca 0‰ after an hour and a minimum  $\Delta^7\text{Li}^{ol-cpx}$  of ca  $-6\%$  after days (Fig. 6b).

Finally, with  $K_D$ ,  $x$ ,  $\beta$ ,  $C_1$  and  $\delta^7\text{Li}$  of the Li reservoir fixed, there is only one rim concentration ( $C_0$ ) that will reproduce a particular Li concentration and  $\delta^7\text{Li}$  at any time  $t$ . However, modelling solutions are non-unique in that assumptions must be made regarding grain-size, Li diffusivity,  $\beta$ , initial composition, etc., and these parameters may be varied in different ways to attain similar modelling results.

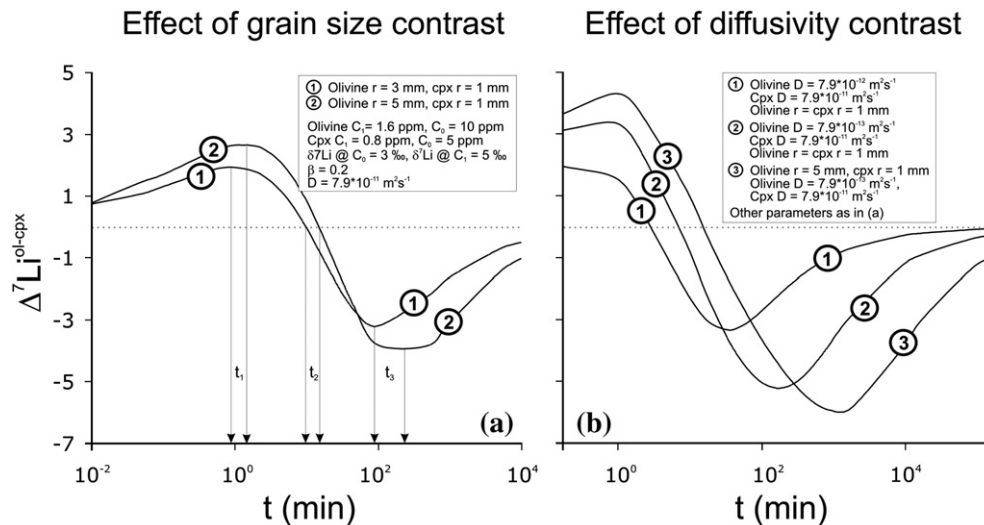


Fig. 6. Time ( $t$ , in minutes) versus  $\Delta^7\text{Li}^{ol-cpx}$  illustrating the effect of (a) different grain sizes where curve 1 represents a 3:1 ratio of grain size between olivine and clinopyroxene, whereas curve 2 represents a 5:1 ratio, (b) different Li diffusivities on intermineral Li isotopic fractionation between olivine and clinopyroxene, where Li diffusivity in olivine is one order of magnitude lower than clinopyroxene for curve 1, whereas for curve 2 it is two orders of magnitude lower. Curve 3 represents a combination of a 5:1 ratio of grain size between olivine and clinopyroxene and two orders of magnitude lower Li diffusivity in olivine than in clinopyroxene.

## 6. Discussion

### 6.1. Elemental equilibrium

An unusual aspect of xenoliths from Tanzania is that, despite the fact that many samples in the present study were subject to carbonatite (Rudnick et al., 1993, 1994) and silicate melt metasomatism (Lee and Rudnick, 1999), most show Li elemental equilibrium, or nearly so (Fig. 1). In contrast, selective Li addition to either olivine or clinopyroxene, depending on whether the melt was silicate or carbonatitic in composition, has been identified as important in creating elemental disequilibrium (Seitz and Woodland, 2000; Woodland et al., 2004) and some other peridotite xenolith suites studied so far (far-east Russia, Rudnick and Ionov, 2007; North China Craton, Tang et al., 2007) show strong olivine-clinopyroxene elemental disequilibrium (Fig. 1a). This suggests that whatever the origin of the observed Li isotope fractionations in Tanzanian samples, it cannot have involved significant recent, selective Li addition.

### 6.2. Relative diffusivities of Li in peridotite minerals

Constraints on the diffusivity of Li in mantle minerals under varying conditions are as yet scarce; to date, only the diffusivity of Li in diopside has been experimentally investigated (Coogan et al., 2005). Since it has been argued that Li may substitute for the similarly sized major cations Mg and Fe in peridotite minerals (Eggins et al., 1998), it might appear reasonable to assume that the relative interdiffusivity of Fe–Mg in olivine, orthopyroxene and clinopyroxene can be used as a proxy for the relative diffusivity of Li in these minerals. It is known that Fe–Mg interdiffusion in olivine far exceeds that of clinopyroxene (Dimanov and Sautter, 2000; Klügel, 2001) and that the Fe–Mg interdiffusivity in clinopyroxene is similar to that of orthopyroxene at 1200 °C, but lower by 1 to 2 log units at 900 °C (Klügel, 2001, and references therein). These relative diffusivities also apply to hydrogen (Demouchy et al., 2006), which, like Li, is a singly charged light element and should be a good proxy for the behaviour of Li. However, in several empirical studies it was inferred that Li diffuses faster in clinopyroxene than in olivine (Jeffcoate et al., 2007; Rudnick and Ionov 2007; Parkinson et al., 2007) and that Li diffusivity in olivine is similar to Fe–Mg interdiffusivity in that mineral (Kaesler et al., 2007), which is  $\sim 10^{-16} \text{ m}^2\text{s}^{-1}$  at 1100 °C (Klügel, 2001) compared to  $4.4 \times 10^{-12} \text{ m}^2\text{s}^{-1}$  for clinopyroxene at the same temperature (Coogan et al., 2005).

Some insight into the diffusivity of Li in olivine can be gleaned from the results of the Labait xenoliths (Aulbach et al., 2008). Here, good correlations between Mg#, Li ppm and  $\delta^7\text{Li}$  in olivine were interpreted to reflect mixing between ancient lithospheric mantle and a metasomatic melt that was Fe- and Li-enriched and isotopically heavy (Aulbach et al., 2008). Thus, the olivines retain their pre-entrapment Li systematics. In contrast, Li in clinopyroxene from the Labait peridotites displays no correlations, suggesting that Li in the clinopyroxene was disturbed during xenolith entrainment by the host basalt. Assuming a temperature of 1300 °C (for the host basalt) and using the appropriate diffusivity for Li in clinopyroxene ( $7.9 \times 10^{-11} \text{ m}^2\text{s}^{-1}$ ; from Coogan et al., 2005), we calculate a range of concentrations and (magma residence) times that will reproduce the observed Li and  $\delta^7\text{Li}$  of the clinopyroxene. We then use these parameters to determine the maximum diffusivities in olivine that would result in no change in Li (see Appendix 3). This modelling approach suggests Li diffusivity in olivine is at least two orders of magnitude smaller than in clinopyroxene.

### 6.3. Kinetic Li isotope fractionation in the mantle: examples from Tanzania

Lithium isotope fractionation in mantle xenoliths due to older enrichment events or to infiltration of melt during residence in the host magma has been described in most studies on peridotite

xenoliths published to date (Jeffcoate et al., 2007; Rudnick and Ionov, 2007; Wagner and Deloué, 2007; Tang et al., 2007; Ionov and Seitz, 2008). The latter may be used to estimate the maximum xenolith residence time in the magma (Li geospeedometry: e.g., Coogan et al. 2005; Lundstrom et al. 2005; Jeffcoate et al. 2007).

#### 6.3.1. Metasomatism in the mantle

The trends between Li concentration,  $\delta^7\text{Li}$  and Mg# found for olivines from the Labait peridotites were interpreted to reflect mantle metasomatism well before entrainment in the host basalt (Aulbach et al., 2008). In most cases,  $\delta^7\text{Li}$  in the coexisting clinopyroxene do not correspond to those of olivine, reflecting recent Li ingress in the clinopyroxene. However, in one sample, LB-51, clinopyroxene has high Li concentration (4.4 ppm) and also  $\delta^7\text{Li}$  (4.1) and shows “normal” partitioning ( $^{ol/cpx}K_{\text{D,Li}}=1.1$ ). These relationships suggest that both olivine and clinopyroxene in this sample have equilibrated with a moderately Li-rich, heavy-Li melt, and neither was disturbed by late Li ingress.

In the case of Olmani, most of the olivines have high Li concentrations (2.9 to 4.1 ppm) and are relatively heavy ( $\delta^7\text{Li}=3.3$  to 6.2‰), overlapping  $\delta^7\text{Li}$  values for mantle-derived carbonatites (Halama et al., 2008). Thus, olivines in these samples may have equilibrated with a calcio-carbonatite magma prior to their entrainment in the host basalt. A single olivine from an Olmani peridotite (89-778) with lower Li abundance (2.6 ppm) but very high  $\delta^7\text{Li}$  (+9.3) may require Li addition from a melt having high  $\delta^7\text{Li}$  and moderate Li concentration, perhaps a small volume melt that had lost  $^6\text{Li}$  preferentially to clinopyroxene during very late diffusion (i.e., during entrainment) (Rudnick and Ionov, 2007). Alternatively, olivine in this sample may have lost  $^6\text{Li}$  during later reaction with a fluid/melt having lower Li abundance than the original carbonatitic melt, thus driving the remaining Li to higher  $\delta^7\text{Li}$ .

In contrast to the Labait and Olmani xenoliths, olivines in most Lashaine peridotites have “normal” mantle-like Li systematics and do not appear to have been affected by Li-metasomatism prior to entrainment. Nevertheless, enriched trace element and radiogenic isotope signatures in Lashaine peridotites show that they have been previously metasomatised (Cohen et al., 1984). Either this metasomatism occurred so long ago that diffusion has erased evidence of Li enrichment (Halama et al., 2008), or the melt responsible for the metasomatism did not have a Li concentration and isotope composition inducing Li diffusion between minerals and melt.

#### 6.3.2. Metasomatism during transport in the host basalt

The non-mantle-like  $\delta^7\text{Li}$  and elevated Li abundance in most clinopyroxene from all three localities indicates incipient Li ingress accompanied by strong kinetic Li isotope fractionation, probably during infiltration of melts from the host magma. A number of features suggest a short magma residence time for the xenoliths and only limited Li ingress into clinopyroxene. These include: 1) the preservation of pre-entrapment systematics in most olivines, 2) apparent equilibrium partitioning of Li between olivine and clinopyroxene, and 3) positive  $\Delta^7\text{Li}^{ol-cpx}$ , which is inferred to reflect the effects of delayed Li isotope fractionation in olivine due to its larger grain size and lower Li diffusivity relative to clinopyroxene, which occurs during the initial stages of Li ingress (Fig. 6b). A short magma residence time is also consistent with the volatile-rich and explosive nature of the host magma (melilitite; Dawson, 1992).

Magma ascent rates in garnet peridotite-bearing mafic-alkalic magmas are estimated to be on the order of 0.1- to 10  $\text{m s}^{-1}$  (Spera, 1984); therefore, for xenoliths from this study, which were entrained from ca 50 to 150 km depths, the magma residence time should be on the order of days. This exceeds by far the short apparent magma residence times modelled here (Fig. 3, example 4: one minute to attain the trough composition; compare to measured clinopyroxene shown in Fig. 4b). These short apparent magma residence times may thus reflect late fragmentation of xenoliths in the host magma and late

penetration of melt, which could develop a range of Li concentrations due to interaction with the xenolith. Because at these temperatures kinetic Li isotope fractionation can only persist on the order of minutes, late fragmentation of xenoliths must be followed by quenching in a tephra in order to preserve the fractionation, as opposed to slow cooling in erupted lavas (cf. Ionov and Seitz, 2008). Alternatively, these apparent short residence times may indicate that the Li diffusivity we assumed is too fast and/or initial Li concentrations too high (see Appendices 2 and 3).

Calculated magma residence times depend critically on the Li diffusivity chosen, which in turn hinges on experimental measurements of diffusion in appropriate minerals and knowing the temperature of the host magma and the temperature gradient across the xenolith. In the absence of these data, it is not yet possible to quantitatively estimate magma residence times using Li isotope fractionation. However, once these constraints become available and considering that xenolith fragmentation may have occurred, the longest calculated magma residence time based on Li diffusion for a large xenolith suite where multiple estimates are available may best approximate the minimum “true” value.

Fractionated melts such as natro-carbonatites can have very high Li abundances and have mantle-like  $\delta^7\text{Li}$  (211 to 294 ppm Li,  $\delta^7\text{Li}=3\text{--}5$ ; Halama et al., 2007,2008), similar to the values required to model the Li systematics of some clinopyroxenes (Appendix 3). Interaction of the peridotite xenoliths with carbonatite melts is consistent with the inferred very late carbonate introduction into some Tanzanian peridotites, which attests to the presence of carbonatite liquids (Lee et al., 2000) and with the presence of the world's only active carbonatite volcano, Oldoinyo Lengai, in the vicinity of the xenolith localities investigated here.

### 6.3.3. Subsolidus lithium diffusion

Lithium partitioning between clinopyroxene and plagioclase has been found to be strongly temperature-dependent, with Li preferring clinopyroxene at decreasing temperatures (Coogan et al., 2005). In addition, a study of Li concentrations of inclusions in diamonds has revealed a strong pressure dependence of Li distribution between mantle minerals (Seitz et al., 2003). Therefore, (isothermal) decompression, or (isobaric) heating and cooling, may influence  $K_D$  and could drive redistribution of Li between minerals and hence cause kinetic isotope fractionation.

Ionov and Seitz (2008) recently suggested that slow cooling causes diffusion of Li from olivine into clinopyroxene, and thus could produce isotopically heavy olivines and lighter clinopyroxene. They suggested that the effects are more pronounced in xenoliths contained in lavas,

which cool much more slowly than those deposited in tuffs. However, the Tanzanian xenoliths show evidence for heating immediately prior to their entrainment in the host basalt, which is likely associated with impingement of a plume on the ancient lithosphere. This evidence includes garnet breakdown coronae, Ca increase on orthopyroxene rims (Lee and Rudnick, 1999) and Zr increase on the rims of metasomatic rutiles (Watson et al., 2006). Because of the relatively high diffusivity of Zr in rutile, the latter imply recent heating of the peridotites to temperatures of 1350–1400 °C (Watson, pers. comm.). In addition, all of the samples investigated here come from tuffs or scoria cones and are expected to have cooled rapidly following eruption. Thus the evidence for heating, coupled with the small Li enrichment inferred on the basis of modelling, suggests that the Li isotopic fractionation in the Tanzanian clinopyroxenes is most likely to have been produced by Li ingress from a grain-boundary melt, rather than slow cooling.

### 6.4. General observations and implications for Li isotope fractionation in minerals from peridotite xenoliths worldwide

An evaluation of Li isotope and abundance data for peridotite xenoliths from this study and those previously published (Fig. 4) reveals two general features: (1)  $\delta^7\text{Li}$  in mantle olivines is mostly within the range proposed for the mantle and almost never lighter and (2)  $\delta^7\text{Li}$  in clinopyroxene is mostly lighter and never heavier than the mantle range. Modelling shows that the whole grain Li- $\delta^7\text{Li}$  relationships of olivine and clinopyroxene in most peridotite xenoliths worldwide can be described by five stages or boundary conditions for igneous Li isotope fractionation (Fig. 7): A) incipient Li addition leading to strong kinetic Li isotope fractionation but only slight Li gain, B) intermediate-term Li addition leading to relaxation of Li isotope fractionation and some Li gain, C) long-term Li addition resulting in (near) equilibration with a mantle-like melt ( $\delta^7\text{Li}$  between +2 and +6 – grey field) having moderate Li concentrations, (D) intermediate to long-term Li addition with a residual  $^7\text{Li}$ -rich melt ( $\delta^7\text{Li}>15$ ) with moderate Li concentrations and (E) intermediate-term Li addition from a Li-rich (>100 ppm) melt with mantle-like  $\delta^7\text{Li}$ .

Heavy Li ( $\delta^7\text{Li}>6$ ) in mantle minerals has been suggested to result from Li ingress or precipitation from residual, isotopically heavy melts that have lost  $^6\text{Li}$  during earlier diffusion (Rudnick and Ionov, 2007; Wagner and Deloule, 2007), while  $\delta^7\text{Li}$  at the high end of mantle values (+5 to +6) combined with high Li abundances (>2 ppm), such as seen at Labait, may reflect reaction with Li-rich, plume-derived, isotopically heavy mantle melts (Aulbach et al., 2008). If Li diffusivity in clinopyroxene is faster than in olivine, the general features in the worldwide dataset and modelling suggest that (1) heavy  $\delta^7\text{Li}$  (>4‰ to

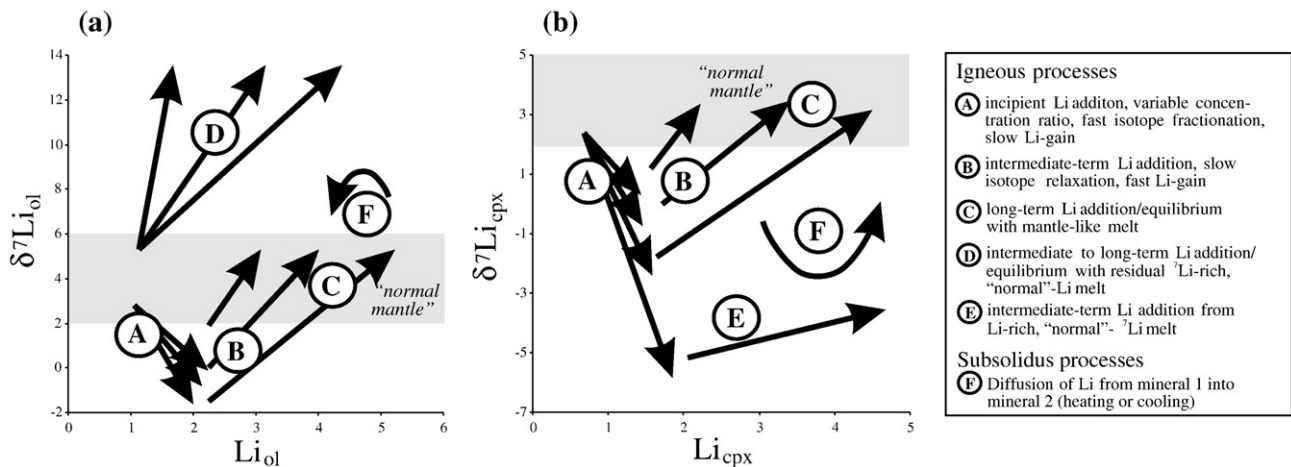


Fig. 7. Schematic representation in Li- $\delta^7\text{Li}$  space of (a) olivine and (b) clinopyroxene of different stages of igneous processes (Li addition) and of subsolidus redistribution of Li from olivine into clinopyroxene. Capital letters denote regions in the diagram according to descriptions given in the right panel.

+6‰) in olivines is due to equilibrium with (isotopically heavy) melts during older metasomatic processes, whereas (2) lighter  $\delta^7\text{Li}$  (<2) in clinopyroxene observed for most samples in the database is due to isotope fractionation during recent Li ingress, probably related to transport in the host magma, but which also may be produced during slow cooling of the xenolith in a lava (Ionov and Seitz, 2008). Clinopyroxene is more susceptible to this process than olivine because of its faster diffusivity and its generally smaller grain size. Thus, Li isotope systematics in peridotite xenoliths likely reflect at least a two-stage process, with olivine showing some capacity to preserve pre-eruptive signatures (which can include original depletion in refractory samples or metasomatic enrichment). Xenolith residence in and interaction with the host melt may not last long enough to allow full Li isotope equilibration in clinopyroxene or corruption of earlier Li systematics in olivine.

The ability of olivine to retain pre-entrainment information with regard to Li concentration and  $\delta^7\text{Li}$  is also illustrated in Figs. 1 and 2 for samples from Tanzania that have previously been described as metasomatised/fertile or refractory based on mineralogy and composition (Rudnick et al., 1993, 1994; Lee and Rudnick, 1999). Olivines in all but one metasomatised sample from Tanzania have higher Li concentrations and  $\delta^7\text{Li}$  than olivines from refractory samples, whereas this relationship breaks down for clinopyroxene and orthopyroxene.

Variations resulting from the intermineral redistribution of Li, e.g., during heating in the host magma or slow cooling in lava-hosted xenoliths are likely (Fig. 6, example F). The interplay between Li diffusion due to ingress from grain boundaries on the one hand, and to intermineral Li redistribution on the other, and attendant isotope fractionation will lead to superimposed effects on Li isotope composition and, perhaps not surprisingly, to a decoupling of Li abundances and isotope compositions in most xenolith suites.

The observations and models discussed above suggest that Li systematics may hold promise for obtaining information from single xenoliths on the nature (mantle metasomatic melts, host melt) and time-scales (pre-eruptive, syn-eruptive) of Li diffusion in the mantle, provided that tighter experimental constraints become available and that samples are quenched upon eruption. Currently, the many unconstrained parameters governing kinetic Li isotope fractionation preclude a quantitative application of Li isotopes to geospeedometry in magma-borne mantle xenoliths, although modelling may be used to qualitatively assess the boundary conditions necessary to obtain the sign and degree of inter-mineral Li isotope fractionation observed in a given xenolith suite.

## 7. Summary and conclusions

We measured  $\delta^7\text{Li}$  of clinopyroxene, orthopyroxene and olivine in variably metasomatised peridotite xenoliths from two lithospheric mantle sections beneath the East African Rift in Tanzania (Lashaine, Olmani) and combined these results with those from the nearby Labait volcano (Aulbach et al., 2008). Peridotite minerals show systematic offsets in their Li concentrations (olivine average: 2.4 ppm, orthopyroxene: 2.0 ppm, clinopyroxene 1.5 ppm) and  $\delta^7\text{Li}$ : olivine contains the heaviest Li (+2.3 to +13.9‰, average +5.0‰), followed by orthopyroxene (−4.1 to +6.5‰, average +0.8‰) and clinopyroxene (−6.7 to +4.1‰, average −1.6‰).

Intermineral Li isotope fractionation in mantle peridotites is ascribed to differential diffusivities of Li in and different grain sizes of mantle minerals, combined with diffusion-driven kinetic Li isotope fractionation. Two main processes, igneous and subsolidus, are proposed to be important in mantle xenoliths and have been qualitatively modelled, awaiting tighter experimental constraints on the parameters governing Li isotope fractionation:

**Igneous processes.** (a) *Precursor metasomatism.* High Li concentrations in both olivine and clinopyroxene in silicate and carbonatite melt-metasomatised minerals from Labait and Olmani and preservation of apparent equilibrium Li partition coefficients attest to older Li addition. In contrast, most peridotites from Lashaine escaped metasomatism,

having primitive mantle-like or depleted Li concentrations. (b) *Entrainment of the xenoliths in the host magma.* Clinopyroxenes in most samples in all three Tanzanian peridotite suites have non mantle-like  $\delta^7\text{Li}$  (<+2), but Li concentrations suggest elemental equilibrium with olivine, consistent with very recent, incipient Li addition, which probably occurred during transport in the host magma. Some clinopyroxene with high Li concentrations (>3 ppm) combined with low  $\delta^7\text{Li}$  (<−3) appear to have interacted very recently with Li-rich (~100 ppm) fluids, perhaps due to xenolith fragmentation upon exsolution of volatile- and Li-rich melts from the host magma.

(2) *Subsolidus processes.* Changes in pressure and/or temperature may lead to intermineral Li redistribution between coexisting minerals and attendant kinetic isotope fractionation. Although cooling has recently been suggested to cause Li diffusion from olivine into clinopyroxene (Ionov and Seitz, 2008), these effects are probably not important in Tanzanian xenoliths, which show evidence for plume-induced heating in the deep lithosphere immediately prior to entrainment and were quenched upon eruption of the host magmas. Hence, for our samples, Li isotope fractionation during Li ingress from a grain boundary melt is more likely to have produced the observed  $\delta^7\text{Li}$  fractionation.

Lithium- $\delta^7\text{Li}$  systematics in peridotite xenoliths worldwide most likely reflect two-stage processes, with olivine capable of preserving a signature of older depletion (in refractory samples) or of (precursory) melt metasomatism with generally “normal” mantle  $\delta^7\text{Li}$  (+2 to +6), while non mantle-like, low  $\delta^7\text{Li}$  in almost all clinopyroxene may reflect Li addition during transport in the host magma. Hidden in these relationships may be small but significant Li isotope fractionations due to subsolidus Li redistribution in response to heating, cooling and/or decompression.

## Acknowledgments

We thank Igor Puchtel for help in the isotope geochemistry lab, and Richard Ash, Bill McDonough and Fang-zhen Teng for assistance with the Nu MC ICPMS. We gratefully acknowledge insightful comments by Thomas Zack and constructive reviews by Michael Seitz, Kari Cooper, and the editor, Maureen Feineman. This work was carried out with support from the NSF (grants EAR-0208012 and EAR-0609689) and while S.A. was the recipient of a Feodor-Lynen fellowship from the Alexander-von-Humboldt Foundation.

## Appendix A. Supplementary data

Supplementary data associated with this article can be found, in the online version, at doi:10.1016/j.chemgeo.2008.07.015.

## References

- Adam, J., Green, T., 2006. Trace element partitioning between mica- and amphibole-bearing garnet lherzolite and hydrous basanitic melt: 1. Experimental results and the investigation of controls on partitioning behaviour. *Contrib. Mineral. Petrol.* 152, 1–17.
- Aulbach, S., Rudnick, R.L., McDonough, W.F., 2008. Li–Sr–Nd Isotope Signatures of the Plume and Cratonic Lithospheric Mantle Beneath the Margin of the Rifted Tanzanian Craton (Labait). *Contrib. Mineral. Petrol.* 155, 79–92.
- Beck, P., Chaussidon, M., Barrat, J.A., Gillet, Ph., Bohn, M., 2006. Diffusion induced Li isotopic fractionation during the cooling of magmatic rocks: The case of pyroxene phenocrysts from nakhlite meteorites. *Geochim. Cosmochim. Acta* 70, 4813–4825.
- Brenan, J.M., Neroda, E., Lundstrom, C.C., Shaw, H.F., Ryerson, F.J., Phinney, D.L., 1998. Behaviour of boron, beryllium, and lithium during melting and crystallization: Constraints from mineral-melt partitioning experiments. *Geochim. Cosmochim. Acta* 62, 2129–2141.
- Brey, G.P., Köhler, T., Nickel, K.G., 1990. Geothermobarometry in 4-phase lherzolites. 1. Experimental results from 10 to 60 KB. *J. Petrol.* 31, 1313–1352.
- Brooker, R.A., James, R.H., Blundy, J.D., 2004. Trace elements and Li isotope systematics in Zabargad peridotites: evidence of ancient subduction processes in the Red Sea mantle. *Chem. Geol.* 212, 194–204.
- Chakraborty, S., 1997. Rates and mechanisms of Fe–Mg interdiffusion in olivine at 980–1300 °C. *J. Geophys. Res.* 102, 12317–12331.
- Chan, L.H., Edmond, J.M., Thompson, G., Gillis, K., 1992. Lithium isotopic composition of submarine basalts: Implications for the lithium cycle in the oceans. *Earth Planet. Sci. Lett.* 108, 151–160.

- Chan, L.H., Gieskes, J.M., You, C.F., Edmond, J.M., 1994. Lithium isotope geochemistry of sediments and hydrothermal fluids of the Guaymas Basin, Gulf of California. *Geochim. Cosmochim. Acta* 58, 4443–4454.
- Chan, L.H., Alt, J.C., Teagle, D.A.H., 2002. Lithium and lithium isotope profiles through the upper oceanic crust: A study of seawater–basalt exchange at ODP Sites 504B and 896A. *Earth Planet. Sci. Lett.* 201, 187–201.
- Chan, L.H., Leeman, W.P., Plank, T., 2006. Lithium isotopic composition of marine sediments. *Geochem. Geophys. Geosyst.* 7 (6), Q06005. doi:10.1029/2005GC001202.
- Chesley, J.T., Rudnick, R.L., Lee, C.T., 1999. Re–Os systematics of mantle xenoliths from the East African Rift: Age, structure, and history of the Tanzanian craton. *Geochim. Cosmochim. Acta* 63, 1203–1217.
- Cohen, R.S., O'Nions, R.K., Dawson, J.B., 1984. Isotope geochemistry of xenoliths from East Africa: implications for development of mantle reservoirs and their interaction. *Earth Planet. Sci. Lett.* 68, 209–220.
- Coogan, L.A., Kasemann, S.A., Chakraborty, S., 2005. Rates of hydrothermal cooling of new oceanic upper crust derived from lithium–geospeedometry. *Earth Planet. Sci. Lett.* 240, 415–424.
- Crank, J., 1975. *The Mathematics of Diffusion*. Clarendon Press, Oxford. 414 pp.
- Dawson, J.B., 1984. Contrasting types of mantle metasomatism? In: Kornprobst, J. (Ed.), *Kimberlites II; the Mantle and Crust–Mantle Relationships*. Elsevier, Amsterdam, pp. 289–294.
- Dawson, J.B., 1992. Neogene tectonics and volcanicity in the North Tanzania sector of the Gregory Rift–Valley – contrasts with the Kenya sector. *Tectonophysics* 204, 81–92.
- Dawson, J.B., Powell, D.G., Reid, A.M., 1970. Ultrabasic xenoliths and lava from the Lashaine volcano, northern Tanzania. *J. Petrol.* 11, 519–548.
- Demouchy, S., Jacobsen, S.D., Gaillard, F., Stern, C.R., 2006. Rapid magma ascent recorded by water diffusion profiles in mantle olivine. *Geology* 34, 429–432.
- Dimanov, A., Sautter, V., 2000. “Average” interdiffusion of (Fe,Mn)–Mg in natural diopside. *Eur. J. Mineral.* 12, 749–760.
- Eggins, S.M., Woodhead, J.D., Kinsley, L.P.J., Mortimer, G.E., Sylvester, P., McCulloch, M.T., Hergt, J.M., Handler, M.R., 1997. A simple method for the precise determination of  $\delta = 40$  trace elements in geological samples by ICPMS using enriched isotope internal standardisation. *Chem. Geol.* 134, 311–326.
- Eggins, S.M., Rudnick, R.L., McDonough, W.F., 1998. The composition of peridotites and their minerals: a laser-ablation ICP–MS study. *Earth Planet. Sci. Lett.* 154, 53–71.
- Elliott, T., Jeffcoate, A., Boumann, C., 2004. The terrestrial Li isotope cycle: light-weight constraints on mantle convection. *Earth Planet. Sci. Lett.* 220, 1–15.
- Farver, J.R., Yund, R.A., Rubie, D.C., 1994. Magnesium grain boundary diffusion in forsterite aggregates at 1000°–1300 °C and 0.1 MPa to 10 GPa. *J. Geophys. Res.* 99, 19809–19819.
- Govindaraju, K., 1995. 1995 working values with confidence limits for twenty-six CRPG, ANRT and IWG–GIT geostandards. *Geostand. Newsl.* 19, 1–32.
- Halama, R., McDonough, W.F., Rudnick, R.L., Keller, J., Klaudius, J., 2007. The Li isotopic composition of Oldoinyo Lengai: nature of the mantle sources and lack of isotopic fractionation during carbonatite petrogenesis. *Earth Planet. Sci. Lett.* 254, 77–89.
- Halama, R., McDonough, W.F., Rudnick, R.L., Bell, K., 2008. Tracking the lithium isotopic evolution of the mantle using carbonatites. *Earth Planet. Sci. Lett.* 265, 726–742.
- Hier–Majumder, S., Anderson, I.M., Kohlstedt, D.L., 2005. Influence of protons on Fe–Mg interdiffusion in olivine. *J. Geophys. Res.* 110, B02202.
- Ionov, D.A., Seitz, H.-M., 2008. Lithium abundances and isotopic compositions in mantle xenoliths from subduction and intra-plate settings: mantle sources versus eruption histories. doi:10.1016/j.epsl.2007.11.020.
- Jagoutz, E., Palme, H., Baddenhausen, H., Blum, K., Cendales, M., Dreibus, G., Spettel, B., Lorenz, V., Wänke, H., 1979. The abundances of major, minor and trace elements in the Earth's mantle as derived from primitive ultramafic nodules. *Proceedings of the Lunar Planetary Science Conference, 10th*, pp. 2031–2050.
- Jeffcoate, A.B., Elliott, T., Kasemann, S.A., Ionov, D., Cooper, K., Brooker, R., 2007. Li isotope fractionation in peridotites and mafic melts. *Geochim. Cosmochim. Acta* 71, 202–218.
- Kaerer, B., Kalt, A., Ludwig, T., 2007. Li, Be, and B abundances in minerals of peridotite xenoliths from Marsabit (Kenya): Disequilibrium processes and implications for subduction zone signatures. *Geochem. Geophys. Geosyst.* 8. doi:10.1029/2006GC001555 Q09013.
- Klügel, A., 2001. Prolonged reactions between harzburgite xenoliths and silica-undersaturated melt: implications for dissolution and Fe–Mg interdiffusion rates of orthopyroxene. *Contrib. Mineral. Petrol.* 141, 1–14.
- Kohlstedt, D.L., Mackwell, S.J., 1999. Solubility and diffusion of “water” in silicate minerals. In: Wright, K., Catlow, R. (Eds.), *Microscopic properties and processes in minerals*. Kluwer Academic Publishers, Dordrecht, pp. 539–559.
- Lee, C.-T., Rudnick, R.L., 1999. Compositionally stratified cratonic lithosphere: Petrology and geochemistry of peridotite xenoliths from the Labait Volcano, Tanzania. In: Gurney, J., Gurney, J., Pascoe, M., Richardson, S. (Eds.), *Proceedings of the 7th International Kimberlite Conference. Red Roof Design cc*, Cape Town, pp. 503–521.
- Lee, C.-T., Rudnick, R.L., McDonough, W.F., Horn, I., 2000. Petrologic and geochemical investigation of carbonates in peridotite xenoliths from northeastern Tanzania. *Contrib. Mineral. Petrol.* 139, 470–484.
- Lundstrom, C.C., Chaussidon, M., Hsui, A.T., Kelemen, P., Zimmerman, A., 2005. Observations of Li isotopic variations in the Trinity Ophiolite: Evidence for isotopic fractionation by diffusion during mantle melting. *Geochim. Cosmochim. Acta* 69, 735–751.
- Magna, T., Wiechert, U., Halliday, A.N., 2006. New constraints on the lithium isotope compositions of the Moon and terrestrial planets. *Earth Planet. Sci. Lett.* 243, 336–353.
- Marks, M.A.W., Rudnick, R.L., McCammon, C., Vennemann, T., Markl, G., 2007. Arrested kinetic Li isotope fractionation at the margin of the Ilímaussaq complex, South Greenland: Evidence for open-system processes during final cooling of peralkaline igneous rocks. *Chem. Geol.* 246, 207–230.
- McDonough, W.F., Sun, S.-S., 1995. The composition of the Earth. *Chem. Geol.* 120, 223–253.
- Möller, A., Mezger, K., Schenk, V., 1998. Crustal age domains and the evolution of the continental crust in the Mozambique Belt of Tanzania: Combined Sm–Nd, Rb–Sr, and Pb–Pb isotopic evidence. *J. Petrol.* 39, 749–783.
- Moriguti, T., Nakamura, E., 1998a. Cross-arc variation of Li isotopes in lavas and implications for crust/mantle recycling at subduction zones. *Earth Planet. Sci. Lett.* 163, 167–174.
- Moriguti, T., Nakamura, E., 1998b. High-yield lithium separation and precise isotopic analysis for natural rock and aqueous samples. *Chem. Geol.* 145, 91–104.
- Nishio, Y., Nakai, S., Yamamoto, J., Sumino, H., Matsumoto, T., Prikhod'ko, V.S., Arai, S., 2004. Lithium isotopic systematics of the mantle-derived ultramafic xenoliths: implications for EM1 origin. *Earth Planet. Sci. Lett.* 217, 245–261.
- Parkinson, I.J., Hammond, S.J., James, R.H., Rogers, N.W., 2007. High-temperature lithium isotope fractionation: Insights from lithium isotope diffusion in magmatic systems. *Earth Planet. Sci. Lett.* 257, 609–621.
- Richter, F.M., Davis, A.M., DePaolo, D.J., Watson, E.B., 2003. Isotope fractionation by chemical diffusion between molten basalt and rhyolite. *Geochim. Cosmochim. Acta* 67, 3905–3923.
- Rudnick, R.L., Ionov, D.A., 2007. Lithium elemental and isotopic disequilibrium in minerals from peridotite xenoliths from far-east Russia: product of recent melt–rock reaction. *Earth Planet. Sci. Lett.* 256, 278–293.
- Rudnick, R.L., McDonough, W.F., Chappell, B.W., 1993. Carbonatite metasomatism in the northern Tanzanian mantle: petrographic and geochemical characteristics. *Earth Planet. Sci. Lett.* 114, 463–475.
- Rudnick, R.L., McDonough, W.F., Orpin, A., 1994. Northern Tanzanian peridotite xenoliths: a comparison with Kaapvaal peridotites and inferences on metasomatic interactions. In: Kimberlites, Related Rocks and Mantle Xenoliths. In: Meyer, H.O.A., Leonardos, O. (Eds.), *Proceedings of the 5th International Kimberlite Conference, Vol. I*, pp. 336–353.
- Rudnick, R.L., Tomascak, P.B., Njo, H.B., Gardner, L.R., 2004. Extreme lithium isotopic fractionation during continental weathering revealed in sapprolites from South Carolina. *Chem. Geol.* 212, 45–57.
- Ryan, J.G., Langmuir, C.H., 1987. The systematics of lithium abundances in young volcanic rocks. *Geochim. Cosmochim. Acta* 51, 1727–1741.
- Seitz, H.M., Woodland, A.B., 2000. The distribution of lithium in peridotite and pyroxenitic mantle lithologies – an indicator of magmatic and metasomatic processes. *Chem. Geol.* 166, 47–64.
- Seitz, H.M., Brey, G.P., Stachel, T., Harris, J.W., 2003. Li abundances in inclusions in diamonds from the upper and lower mantle. *Chem. Geol.* 201, 307–318.
- Seitz, H.M., Brey, G.P., Lahaye, Y., Durali, S., Weyer, S., 2004. Lithium isotopic signatures of peridotite xenoliths and isotopic fractionation at high temperature between olivine and pyroxenes. *Chem. Geol.* 212, 163–177.
- Seyfried Jr., W.E., Chen, X., Chan, L.H., 1998. Trace element mobility and lithium isotope exchange during hydrothermal alteration of seafloor weathered basalt: An experimental study at 350 °C, 500 bars. *Geochim. Cosmochim. Acta* 62, 949–960.
- Spera, F.J., 1984. Carbon dioxide in petrogenesis III: role of volatiles in the ascent of alkaline magma with special reference to xenolith-bearing mafic lavas. *Contrib. Mineral. Petrol.* 88, 217–232.
- Tang, Y.-J., Zhang, H.-F., Nakamura, E., Moriguti, T., Kobayashi, K., Ying, J.-F., 2007. Lithium isotopic systematics of peridotite xenoliths from Hannuoba, North China Craton: Implications for melt–rock interaction in the considerably thinned lithospheric mantle. *Geochim. Cosmochim. Acta* 71, 4327–4341.
- Teng, F.-Z., McDonough, W.F., Rudnick, R.L., Dalpé, C., Tomascak, P.B., Chappell, B.W., Gao, S., 2004. Lithium isotopic composition and concentration of the upper continental crust. *Geochim. Cosmochim. Acta* 68, 4167–4178.
- Teng, F.-Z., McDonough, W.F., Rudnick, R.L., Walker, R.J., Sirbescu, M.-L., 2006a. Lithium isotopic systematics of granites and pegmatites from the Black Hills, South Dakota. *Am. Mineral.* 91, 1488–1498.
- Teng, F.-Z., McDonough, W.F., Rudnick, R.L., Walker, R.J., 2006b. Diffusion-driven extreme lithium isotopic fractionation in country rocks of the Tin Mountain pegmatite. *Earth Planet. Sci. Lett.* 243, 701–710.
- Tomascak, P.B., 2004. Developments in the understanding and application of lithium isotopes in the Earth and planetary sciences. *Rev. Mineral. Geochem.* 55, 153–195.
- Tomascak, P.B., Tera, F., Helz, R.T., Walker, R.J., 1999. The absence of lithium isotope fractionation during basalt differentiation: new measurements by multicollector sector ICP–MS. *Geochim. Cosmochim. Acta* 63, 907–910.
- Tomascak, P.B., Langmuir, C.H., le Roux, P.J., Shirey, S.B., 2008. Lithium isotopes in global mid-ocean ridge basalts. *Geochim. Cosmochim. Acta* 72, 1626–1637.
- Tsuruta, K., Takahashi, E., 1998. Melting study of an alkali basalt JB-1 up to 12.5 GPa: behavior of potassium in the deep mantle. *Phys. Earth Planet. Inter.* 107, 119–130.
- Vauchez, A., Dineur, F., Rudnick, R., 2005. Microstructure, texture and seismic anisotropy of the lithospheric mantle above a mantle plume: Insights from the Labait volcano xenoliths (Tanzania). *Earth Planet. Sci. Lett.* 232, 295–314.
- Wagner, C., Deloule, E., 2007. Behaviour of Li and its isotopes during metasomatism of French Massif Central Iherzolites. *Geochim. Cosmochim. Acta* 71, 4279–4296.
- Watson, E.B., Baxter, E.F., 2007. Diffusion in solid–Earth systems. *Earth Planet. Sci. Lett.* 253, 307–327.
- Watson, E.B., Wark, D.A., Thomas, J.B., 2006. Crystallization thermometers for zircon and rutile. *Contrib. Mineral. Petrol.* 151, 413–433.
- Woodland, A.B., Seitz, H.-M., Yaxley, G.M., 2004. Varying behaviour of Li in metasomatised spinel peridotite xenoliths from Western Victoria, Australia. *Lithos* 75, 55–66.
- Zack, T., Tomascak, P.B., Rudnick, R.L., Dalpé, C., McDonough, W.F., 2003. Extremely light Li in orogenic eclogites: The role of isotope fractionation during dehydration in subducted oceanic crust. *Earth Planet. Sci. Lett.* 208, 209–290.